NPL
National Physical Laboratory

Report

NPL REPORT ENG 8

Overview of tomography techniques to measure wafer thickness in MEMS structures

Andy Robinson & Richard Leach

June 2008

NOT RESTRICTED

National Physical Laboratory | Hampton Road | Teddington | Middlesex | United Kingdom | TW11 0LW
Switchboard 020 8977 3222 | **NPL Helpline** 020 8943 6880 | **Fax** 020 8614 0446 | **www.npl.co.uk**

Department for **Innovation, Universities** & **Skills**

Overview of tomography techniques to measure wafer thickness in MEMS structures

Andy Robinson & Richard Leach

Industry and Innovation Division

ABSTRACT

Possible metrology solutions to the industrial requirement for the measurement of the wafer thickness and internal structure of MEMS sensors are investigated in this report. A range of optical and electrical techniques is reviewed and optical coherence tomography is recommended as the most suitable technique. Optical coherence tomography is considered from a theoretical perspective and a range of system designs and commercially available instruments are discussed. OCT images of a MEMS sensor are included as proof of concept. Finally recommendations are made for further research in image processing area in order to obtain sub-micrometre axial resolution for MEMS measurement.

ISSN 1754-2987

National Physical Laboratory
Hampton Road, Teddington, Middlesex, TW11 0LW

Approved on behalf of the Managing Director, NPL, by Mark Gee, Knowledge Leader,
Engineering Measurement Team, Industry and Innovation Division

Contents

Table of Figures

Table of Tables

1 INTRODUCTION

In 2006 an NPL review [1] investigated the metrology requirements for the manufacture of MEMS sensors. One of the recurring themes was the need to measure the wafer thickness and internal structure of MEMS devices. Following this review a project was undertaken in the 2005-2008 NMS Engineering Measurement Programme to focus on the measurement of wafer thickness and to develop an instrument capable of addressing this need. The outcome of the project is the main focus of this report.

Wafer thickness is routinely measured in the semiconductor industry and in this context refers to whole wafers, which are measured for warp, bow, flatness, etc., prior to being manufactured into semiconductor devices. In the context of MEMS, wafer thickness can refer to not just the thickness of the starting wafer, but in a multi-layered structure, to the thicknesses of the individual layers. Therefore, there is some ambiguity in the use of the terminology in this report depending on the context in which it is used.

This report begins with a detailed analysis of the industrial need to measure wafer thickness including two specific examples. A key aim of this report is to review suitable tomographic methods and to identify the best-suited method for the single sided measurement of silicon wafers. Most well-known, non-contact, single-sided measurement methods and instruments are discussed in chapters 4 and 5. A more detailed treatment of optical coherence tomography (OCT), as the best-suited technique to measure wafer thickness, is discussed in chapter 6. Finally the report concludes by outlining some proposals for further work.

2 INDUSTRIAL REQUIREMENTS

2.1 METROLOGY FOR MEMS

The MEMS market is driven by demand for smaller, cheaper, more versatile and more reliable integrated devices. New developments rest firmly on the semiconductor industry's know-how of silicon wafer production. New metrology systems for the control and monitoring of MEMS fabrication are in demand due to the rapid pace of progress and the broadening range of MEMS applications [2]. However, the MEMS fabrication industry suffers from the lack of rapid non-destructive instruments to perform wafer tests. Current techniques in the semiconductor industry involve layer separation, prior to examination using the scanning electron microscope (SEM). Although the SEM provides sufficient imaging resolution on the layer's

surface, preparing a wafer for SEM inspection is a slow, and often destructive process. Moreover, layer separation is not suitable to the functional inspection of MEMS devices.

MEMS technology is based on creating task-specific three-dimensional functional structures within a wafer consisting of silicon and other compound materials. The thickness of MEMS wafers is in the region of 50 μm to 500 μm, while the thinnest layers within silicon MEMS wafers are in the region of 1 μm.

In the MEMS industry, there is currently a need to measure *in situ* the thickness of the layers of a MEMS wafer immediately after fabrication. Early detection of a fabrication fault could save the MEMS industry substantial costs since the MEMS packaging process can account for around 90% of the cost of the device [1].

2.2 WAFER THICKNESS

There are three general areas where current methods of measuring wafer thickness are inadequate:

1. where the wafer can only be accessed from one side – so the thickness cannot be measured using a conventional probing technique;
2. where probing techniques are not fast enough to enable in-process inspection;
3. where thickness of sub-structure needs to be resolved.

Thickness measurement techniques divide into two broad groups, contact and non-contact methods. A contact method may be of limited use as it would be difficult to resolve MEMS structures that are internal to the wafer. A contact method could also damage fragile, surface MEMS structures and might be unable to spatially resolve high aspect ratio features. The preferred method must, therefore, be non-contact.

Where the wafer can only be accessed from one side, the light source and the detector have to be positioned on the same side. Therefore, the required MEMS thickness measurement method should have the capability to measure the depth of each transition between layers based on the detection of reflections within the wafer. This is effectively a tomographic method.

Full-field inspection of an entire MEMS wafer is not necessarily required. Thickness at strategic locations within a MEMS structure (for example, a diaphragm) may be sufficient. Existing thickness measurement techniques only have the capability to deliver an averaged thickness and

thickness is not resolved laterally. For the purpose of imaging MEMS, an inspection method would be required to provide lateral and depth resolutions of the order of a few micrometres and it should be traceable to national length standards. The method should be able to cope with high aspect ratio structures (HARs) that are typical of MEMS devices. The method's angle of incidence should preferably be normal to the MEMS wafer surface to guarantee access to recessed surface structures.

2.3 CASE STUDIES

The industrial requirements for wafer thickness measurement are illustrated in the following case studies.

2.3.1 Resonant Pressure Transducer (RPT) - GE Sensing.

GE Sensing, formerly Druck, are the UK's foremost MEMS manufacturer. GE is currently developing the Trench Etched Resonant Pressure Sensor (TERPS), see Figure 1. A resonant pressure sensor measures changes in the natural frequency of a resonator as a diaphragm deflects with pressure. The earlier generation of resonant sensor, the Resonant Pressure Transducer (RPT), see Figure 2, is excited electrostatically at 30 kHz. The RPT uses a closed loop feedback system and the supply voltage is monitored to keep the device at resonance from which the pressure measurement is derived. Diaphragm thickness is important to the functioning of the sensor. It is not clear to the manufacturer, whether variations in diaphragm thicknesses are caused by non–uniformity of the wafer or non-uniformity of the etch rate.

The operation of a resonant sensor depends on the successful formation of the diaphragm during the MEMS fabrication. Controlling the diaphragm's thickness immediately after fabrication would be desirable for the early identification of defects.

In this example, the diaphragm is recessed and both sides of the wafer must be accessible to perform a thickness measurement. In a production environment, however, the back of the wafer is not easily accessed, as this would require time-consuming and difficult manipulation of the wafer.

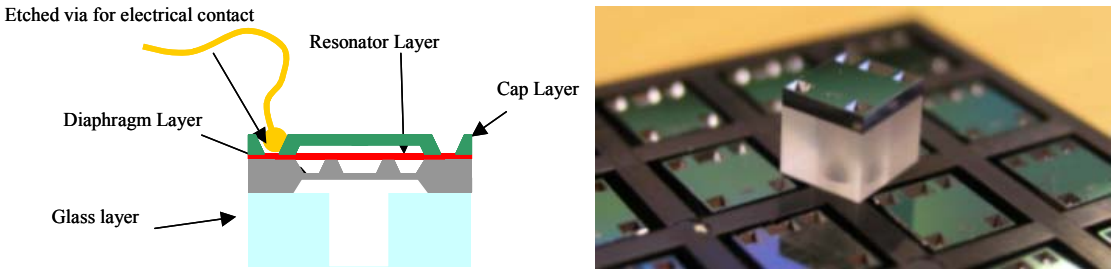

Figure 1. Left, schematic showing the layers for the TERPS. Right, photograph of the finished TERPS. (courtesy GE Sensing)

Figure 2 (left) shows a silicon wafer containing 256 pressure sensors. The blue squares show test points on the wafer where amongst other tests the overall thickness is measured using a contact probe. If the thickness is out of tolerance at one of these test points it is likely that the whole wafer will be scrapped. A quicker method of measuring thickness would enable each device to be individually measured eliminating the potential of scrapping good parts.

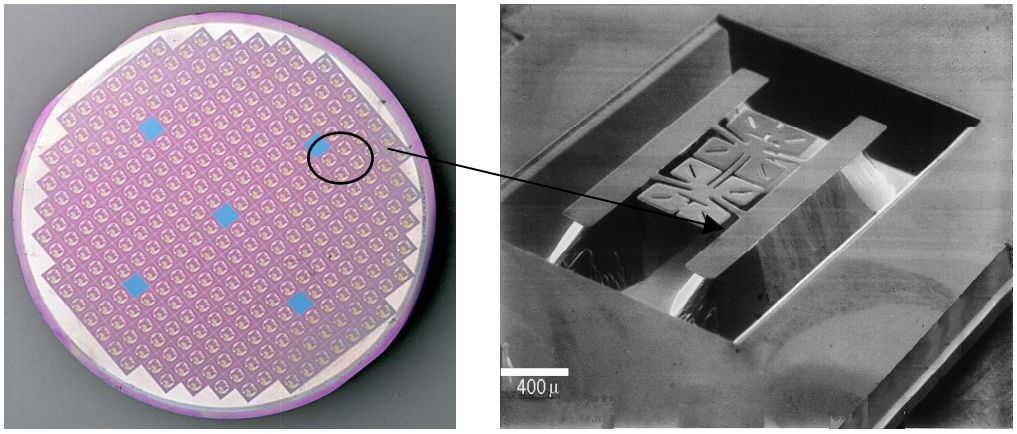

Figure 2. Left, pressure sensors on a silicon wafer. Right, micrograph of the resonator. (courtesy GE Sensing)

During the etch process any imperfections in the silicon can cause pyramid-like structures to grow on the surface. Over a certain size these pyramids can cause the pressure sensor to fail. At present each device goes through a 100% visual inspection by a trained operator to detect these problematic structures. A method of checking the top and bottom surfaces of the diaphragm layer automatically would be very beneficial.

2.3.2 Deep reactive- ion etched wafer - BAE Systems

BAE Systems have a requirement to measure the starting thickness and variations in thickness across a deep reactive-ion etched (DRIE) 100 µm thick silicon wafer. In many applications the frequency and performance of the device is linked to the wafer thickness. In addition to thickness, there is a need to measure high aspect ratio structures on the surface. An example

would be a trench of 10 µm width (see Figure 3), where the aspect ratio of the trench (10:1) prevents the depth being measured for deep etches using optical surface measuring techniques.

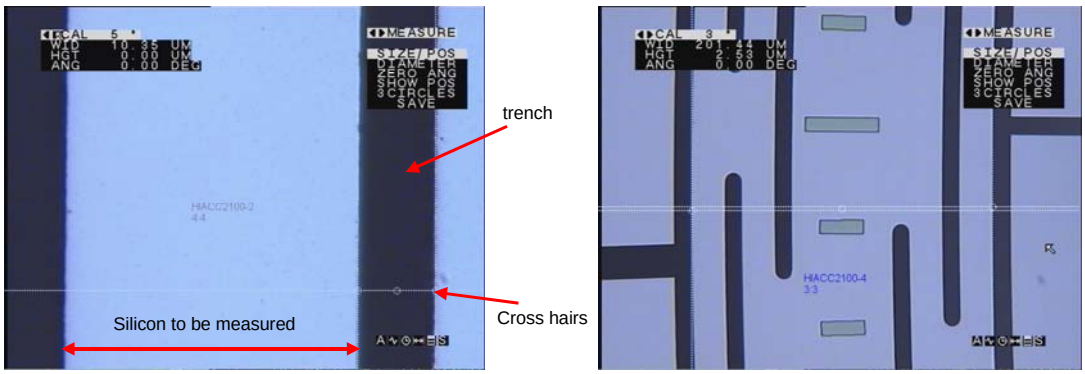

Figure 3. Two images showing typical structures and dimensions requiring measurement at BAE. (courtesy BAE systems)

2.4 SUMMARY OF THICKNESS MEASUREMENT REQUIREMENT

The requirements for an instrument to measure wafer thickness are summarised below. It should

- use a single sided method;
- have a vertical resolution < 1 µm;
- have a lateral resolution ~10 µm;
- have a depth range > 200 µm;
- be silicon compatible;
- have a scan speed suitable for industrial application.

In addition to wafer thickness several other measurement challenges, such as defect detection and high aspect ratio structures (HARS), have been identified by the authors. These will also be considered, in order that any potential solution can have the maximum versatility.

3 OPTICAL PROPERTIES OF SILICON

Silicon is the second most abundant element in the earth's crust (25.7%) and its major contribution to the world economy has resulted from the use of pure silicon wafers in the semiconductor industry. Due to its availability, economies of scale and its ability to incorporate electronic functionality, silicon has become the material of choice in many MEMS applications.

This section covers some of the optical properties of silicon that need to be considered when assessing any suitable measurement technique.

3.1 ABSORPTION AND TRANSMISSION

The absorption coefficient of silicon is a function of wavelength, especially between the visible range (complete opacity) and the infrared range (complete transparency) [3-5]. Figure 4 shows the transmission spectrum for silicon. Transmission can occur for wavelengths above 1.1 μm. This corresponds with the infrared region of the electromagnetic spectrum.

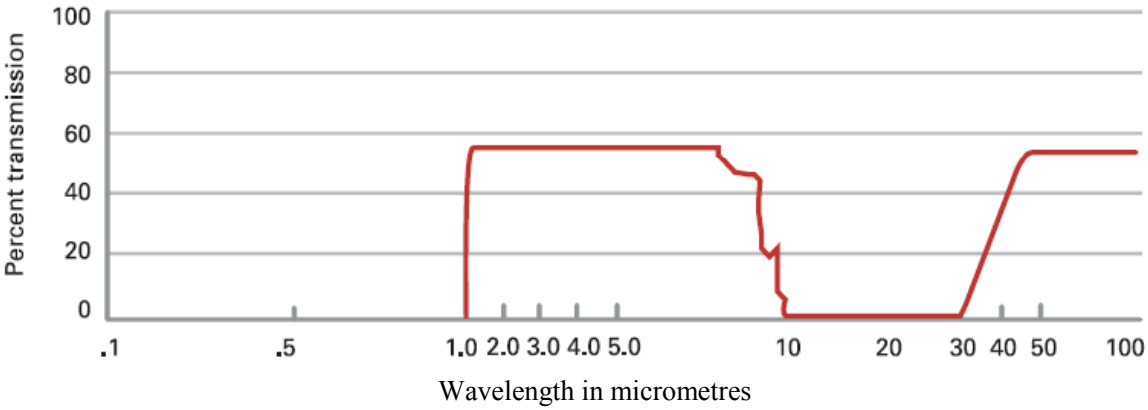

Figure 4. Transmission spectrum of silicon.

Variations of absorption will reduce the bandwidth and reshape the spectral profile of an infrared illumination source, therefore, increasing its apparent coherence length and consequently the axial resolution. The refractive index of silicon also varies as a function of wavelength. For light of wavelength 1.1 μm the refractive index is approximately 3.5.

3.2 DISPERSION

Since silicon is a highly dispersive material in the near infrared region, different wavelengths will travel through at different phase velocities, with the negative effect of extending the coherence length of the source. Group velocity dispersion leads to a depth-dependant loss of optical resolution.

4 REVIEW OF POTENTIAL MEASUREMENT TECHNIQUES

In this section some potential measurement techniques for the measurement of wafer thickness in MEMS structures are reviewed.

4.1 LOW COHERENCE INTERFEROMETRY

Low coherence interferometry (LCI) is a commonly used optical profiling technique for the measurement of roughness and surface topography. [6-9]. LCI is a non-contacting, non-destructive method that is capable of scanning whole wafers to sub-nanometre axial resolutions.

Typically in an interferometer, a light wave is split into two parts, which travel different paths and the waves are then recombined to create interference. A schematic of a coherence scanning interferometer is shown in Figure 5. A polychromatic source is divided by a beam splitter, producing two beams – one travelling to a reference mirror, the other to the sample. The two beams recombine at the detector. Due to the low coherence of the source, interference will only be produced when the two path lengths match to within the coherence length of the source. Therefore, by scanning the reference mirror, the position of the reflection surface on the sample can be determined very accurately. The coherence peak of the interferogram, the point of highest fringe contrast, can be determined and is the point where the rate of change of phase is zero, known as the stationary phase point [10-12].

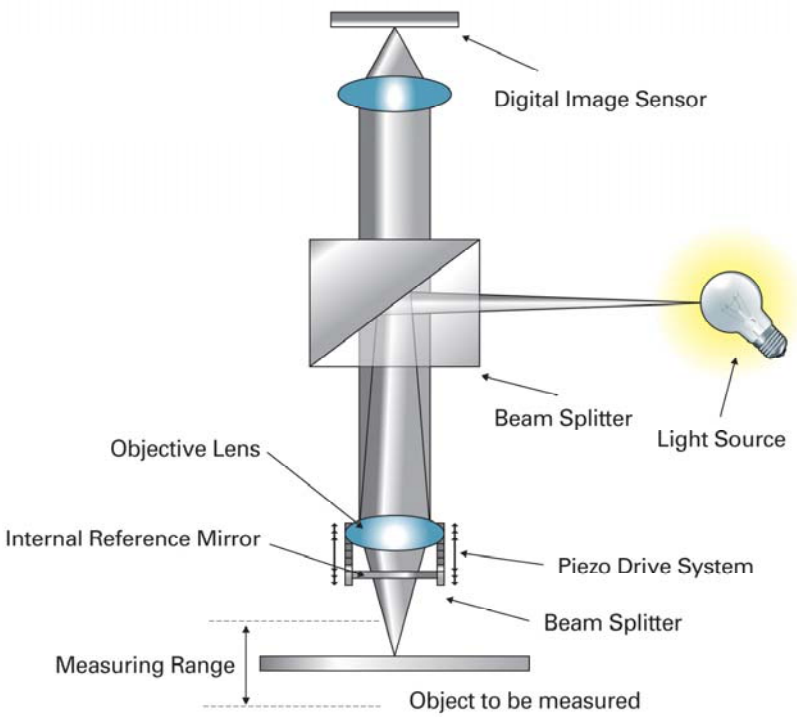

Figure 5. A typical CSI system based on a Mirau interferometer.

LCI is most often exploited to construct surface height maps of a reflecting (or partially reflecting) sample achieving sub-nanometre axial resolution. In this context, LCI is often called

coherence scanning interferometry (CSI).[1] Polychromatic light is used rather that monochromatic light because it has a shorter coherence length. Measurement methods based on LCI have the advantage over 'classical' laser interferometry [13] of completely eradicating the phase unwrapping ambiguity inherent to monochromatic interference, because interference only occurs within the coherence envelope. Figure 6 shows a picture of a Taylor Hobson coherence scanning interferometer at NPL. Coherence scanning interferometery has also been applied to the measurement of transparent thin films [14-15].

Figure 6. A coherence scanning interferometer.

Figure 7 shows an image of the surface of a MEMS pressure sensor taken using a coherence scanning interferometer.

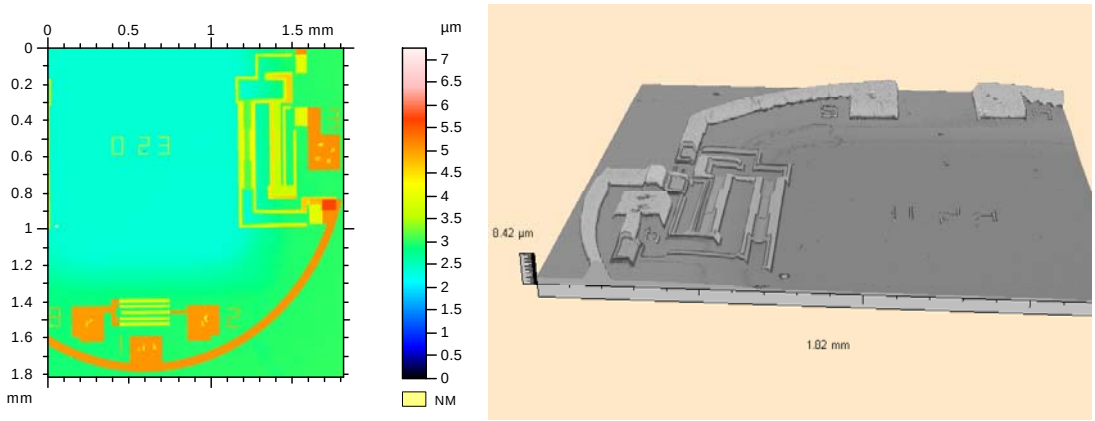

Figure 7. A coherence scanning interferometer.

[1] Coherence is the measure of the average correlation between the value of a wave at a pair of times, separated by a given delay. Temporal coherence characterises how well a wave can interfere with itself at a different time.

LCI has been applied to the problem of thickness measurement by combining two instruments to enable a double-sided measurement [16-17]. Each instrument can measure the topography of one side of the artefact and by using an interferometer to measure the distance between a datum surface on each of the two instruments, an absolute thickness measurement can be obtained. This system design is quite challenging to realise, requiring accurate alignment of each instrument and the measurement artefact.

Although it is intrinsically linked to the usage of a polychromatic source, the concept of LCI is not restricted to visible light. Infrared LCI takes advantage of the partial transparency of specific materials like biological tissues and silicon-based materials. Infrared LCI is more generally called optical coherence tomography (OCT) and its main application is currently medical imaging.

By applying OCT to silicon wafers, it is possible to determine the thickness of each constituting layer. Potentially this could resolve HARs typical in MEMS devices, in all three dimensions.

4.2 CONFOCAL MICROSCOPY

A confocal microscope uses a pinhole in the conjugated focal plane to block unwanted, out-of-focus light from the sample that would normally produce blur. As a result, confocal microscope images are sharper (less blur means higher spatial resolution) than images obtained using a conventional microscope with equivalent magnification [18]. Figure 8 shows the basic design of a confocal microscope.

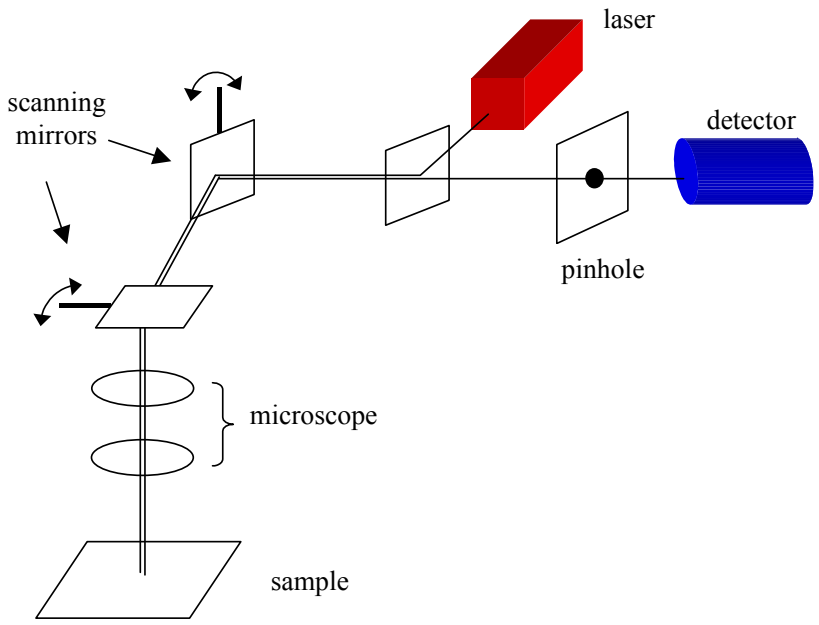

Figure 8. A typical design for a confocal microscope.

The disadvantage of confocal microscopy is that image construction is not immediate compared to conventional microscopy. Since the pinhole only permits collection of light from a single specific location in the sample under observation, the confocal image (effectively a 2D slice) must be built-up by raster scanning the sample. Confocal microscopy is also capable of building 3D images, providing that the sample or the pinhole altitude can be controlled. The 3D image can be built layer by layer by moving the focal plane using a motorised drive. Instrument manufacturers report resolutions in the order of a few hundred nanometres [19-22].

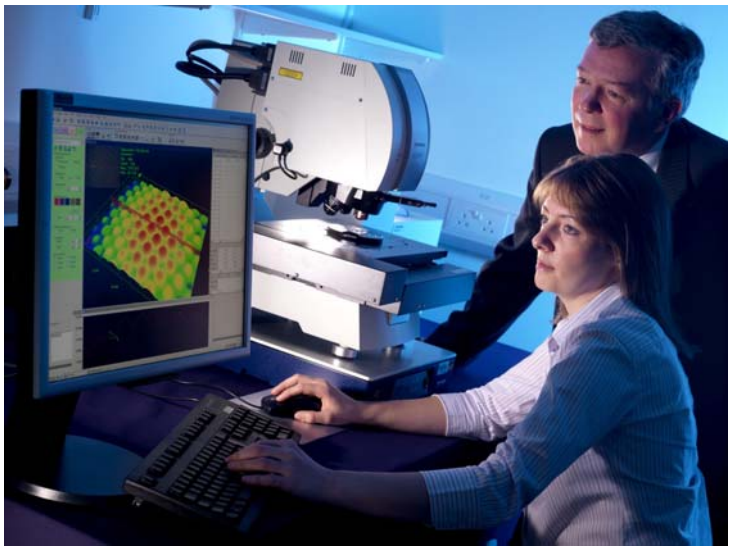

Figure 9. NPL's confocal microscope. (Olympus LEXT)

A particular subset of confocal microscopy is the confocal chromatic sensor. This works as for a classical confocal microscope with the addition of a spectrometer to analyse the spectral content of the light beam. In a chromatic optical system, the position of the image of any given point source depends on the wavelength of the light beam. For a polychromatic light beam, the chromatic optical system exhibits a continuum of images corresponding to the spectral content of that beam. The focussed wavelength will have the highest peak. The advantage of this system is that there is no need to scan normal to the surface. The vertical measurement range is given by the axial chromatic dispersion observed between the shortest and longest wavelengths. Typically a range from micrometres up to millimetres can be achieved [23-24].

Confocal microscopy is a successful technique for the surface examination of semiconductor wafers but confocal microscopes generally are large and heavy instruments (comprising of a conventional microscope, confocal system, video camera, laser light source and control electronics) that are not easily adapted to production environments.

Commercially available confocal microscopes (Olympus, Nikon, Zeiss, Leica) [19-22] are expensive and complex systems based on high-quality research microscopes (Figure 9).

In reflectance mode, the detector of a confocal microscope measures backscattered light intensity at the same wavelength as the source. Consequently any wavelength that will partially reflect from the sample is usable, and in particular infrared can be chosen for the tomographic inspection of silicon wafers. In the last decade, confocal microscopy has been adapted to IR light to resolve embedded defects in silicon wafers [25-26].

Confocal microscopy has similarities to optical coherence tomography. Both methods are able to select the depth of the observation location within a sample, and both methods have the same disadvantages of producing a single point datum. Both methods can deliver micrometre range axial and lateral resolutions. However, OCT has an advantage of being less complex as a microscope is not required.

In the semiconductor industry, confocal infrared microscopy (CIM) is progressively being adopted as a cheaper and quicker alternative to wafer inspection techniques based on scanning electron microscopy, the current preferred method for surface imaging. Although CIM does not provide the same imaging clarity and resolution as SEM, CIM permits an early diagnostic of the wafer by imaging through the different layers in order to spot defects.

4.3 ELLIPSOMETRY

Ellipsometry is a powerful optical technique that measures the change in polarisation on reflection and is used in the measurement of thin films and multi-layer semiconductor structures. Linearly polarised light is reflected from the sample, and on reflection becomes elliptically polarised. From the shape of this polarised ellipse the properties of the sample including thickness, dielectric function and refractive index can be determined [27-28]. The basic setup is shown in Figure 10.

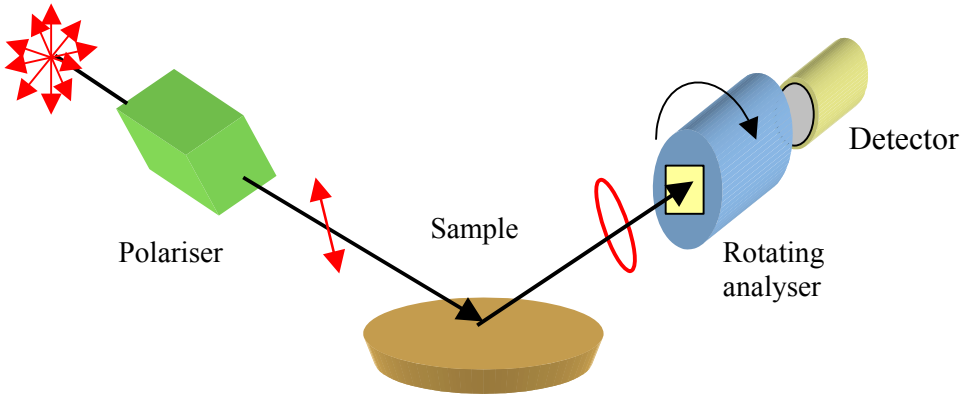

Figure 10. Schematic of an ellipsometer.

Variable angle spectroscopic ellipsometry (VASE) can be used to acquire experimental data over a wide spectral range and a number of different angles of incidence. This means that a large amount of data is collected improving the fitting process, a significant improvement on earlier systems, which operated at single wavelength and angle.

Ellipsometry is a non-contact, single sided measurement and can achieve sub-nanometre resolution. It is commonly applied to films less than 5 μm thick [29], so for the purposes of measuring wafer thickness in MEMS devices its usefulness may be limited. There are many manufacturers of commercial ellipsometers. Figure 11 shows a picture of NPL's ellipsometer (J A Woollam) [30].

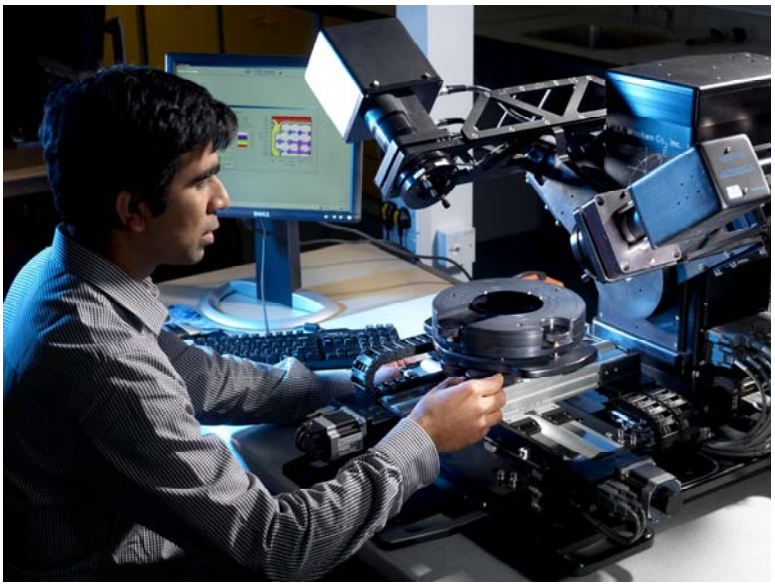

Figure 11. An ellipsometer at NPL.

4.4 SPECTRAL REFLECTOMETRY

Normal–incidence spectral reflectometry measures the intensity of light reflected from a surface [31]. Like ellipsometry, it is a technique suited to the study of thin films and atomic layer resolution is achievable.

Thickness information is contained within the interference fringes of the reflected spectrum. The layers of the sample form a resonant cavity enabling many optical paths to interfere with each other, fringes appear in the measured spectrum of reflected light. The phase of these spectral fringes is a function of wavelength, sample refractive index and sample thickness. If the refractive index of the sample is known, thickness can, therefore, be extracted from an analysis of the fringe period.

The total reflectance spectrum method uses the Fresnel analysis of the multiple-reflection interferences within a silicon wafer illuminated over the visible to near-IR range. The corresponding total reflectance spectrum contains information relating to the wafer surface roughness and wafer thickness.

The approach taken by Sopori *et. al.* [32-36] to measure the thickness of solar cell wafers is to infer the thickness by interpolating a measured total reflectance spectrum against, previously calculated spectra of neighbouring thickness values. A wide angular distribution of light illuminates the sample and the reflected component normal to the sample is measured. A minimum reflectance occurs at a wavelength, which can be related to the film thickness according to the equation

$$t = \frac{\lambda_0}{4n} \qquad (1)$$

where t is the thickness of the film, λ_0 is the wavelength at which the reflectance minima occurs, and n is the refractive index of the film.

Based on this analysis, software algorithms can calculate the theoretical total reflectance spectrum of a hypothetical wafer given its thickness, refractive index, absorption coefficient, extinction coefficient and illumination bandwidth. This technique, aimed at the measurement of an average thickness over a few square centimetres, is based on the measurement of total reflectance spectrum at normal incidence to the wafer surface, itself illuminated through a very

wide angle of incidence from random directions. This is a departure from conventional small-beam reflectometry.

If the surface roughness of the wafer under test has been previously characterised, deconvolution of thickness information is simply based on the measurement of reflectance at a single wavelength in the near-IR band, and interpolation with pre-calculated spectra, which can all be performed very rapidly.

Although this measurement method is fast and single-sided, with sub-micrometre spot size and sub-nanometre axial resolution, the technique can only be applied to thickness below a few micrometres making it of limited interest for thickness measurement of MEMS wafers [37-39].

4.5 FOURIER TRANSFORM INFRARED SPECTROSCOPY

Fourier transform infrared spectroscopy (FTIR) is an interferometric spectroscopy method, and was developed to measure spectral absorbance (or reflectance) in the near and mid infrared regions. FTIR is of particular interest to chemists who can identify complex molecules according to their IR spectral absorbance signatures. (Specific molecular bonds have specific IR absorption energies.)

The basic setup for an FTIR system is shown in Figure 12. The technique can work in transmittance or reflectance modes. There are two ways in which FTIR can be used to measure wafer thickness. Using a low coherence source the distance can be measured between the primary and secondary interferograms. This is similar in principle to time domain OCT. Alternatively the spectral output of the signal can be analysed. The interferogram is Fourier-transformed to reveal the absorbance spectrum of the sample. The wavelengths at which maximum interference occurs will be related to the thickness and refractive index of the sample. In this respect it is similar to spectral reflectometry.

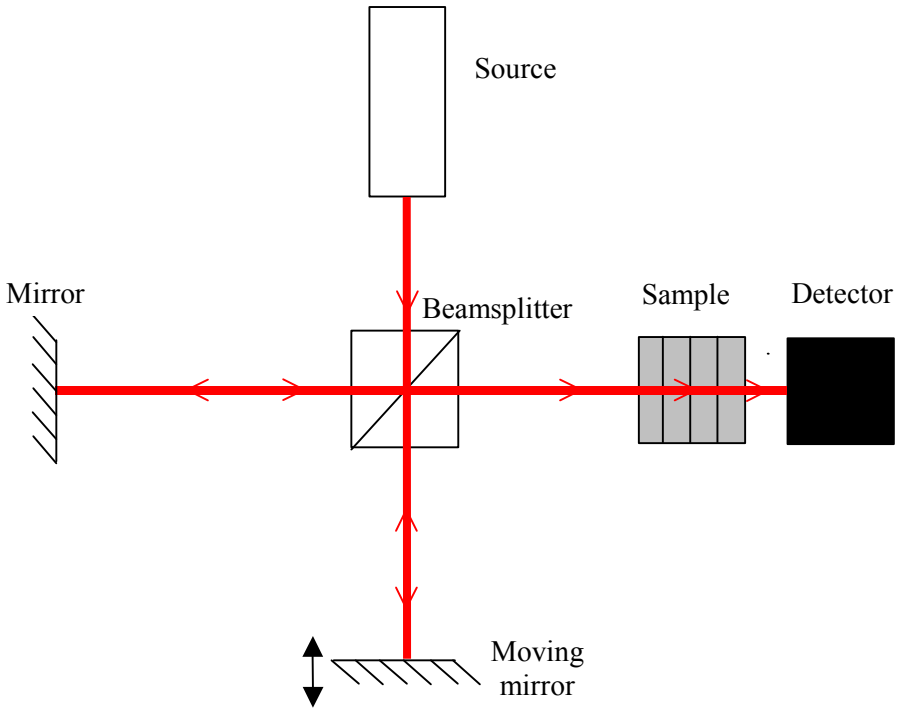

Figure 12. A typical design for Fourier transform infrared spectroscopy.

FTIR is commonly used in the Semiconductor industry to measure a range of properties including film thickness. Themo Scientific [40] are one producer of such instruments. The specification of the ECO 3500 FT-IR metrology tool is listed in Table 1. The lateral resolution of the instrument is not given in the Table. The lateral resolution is dependant on the optics used and with a small spot size (~10 μm) a high-resolution map of the sample could be produced.

Table 1. Specifications for the ECO 3500 (Thermo Scientific)

ECO 3500 FT-IR specifications	
Range	0.3 μm –7.5 μm
Precision	0.002 μm
Accuracy	0.05 μm
Throughput	Up to 140 wafers per hour (300 mm wafers)

4.6 CAPACITANCE

Capacitance measurement can be used to measure wafer thickness by a comparative technique. By measuring the capacitance of a wafer of known thickness the thickness of an unknown wafer can be accurately measured by comparison. The basic principle is shown in Figure 13.

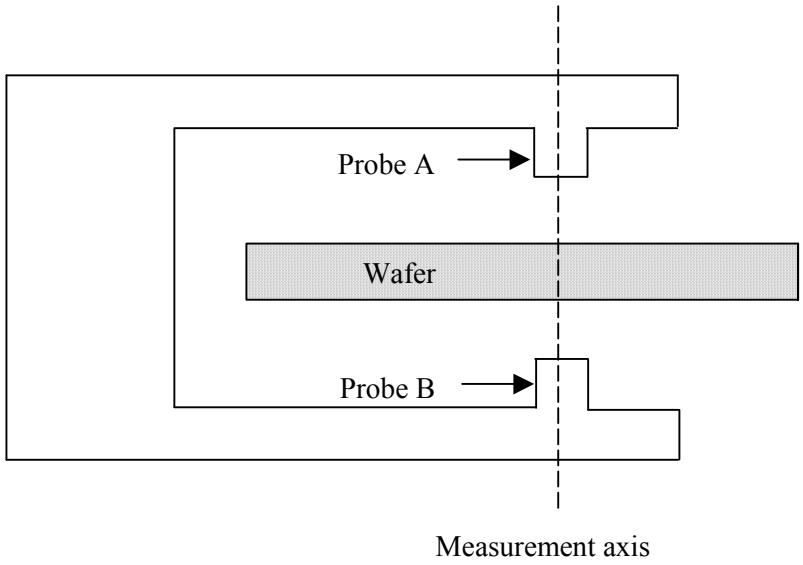

Figure 13. A schematic of a capacitance probe instrument for the measurement of wafer thickness.

Capacitance measurement can also be used to determine wafer bow, warp and flatness. The technique is best suited to a plain wafer and cannot identify or measure thicknesses of multiple layers contained in a MEMS device. This technique is a non-contact method, and access is required to both sides of the artefact. A calibrated reference artefact is also required for traceability.

MTI instruments [41] produce a range of capacitance measurement instruments for the semiconductor industry. The performance of one instrument - the Proforma 300 - is summarised in Table 2 giving an indication of the capability of a capacitance measurement technique.

Table 2. Specifications for the Proforma 300 (MTI instruments)

Proforma 300 - specifications	
Wafer size	50 mm – 300 mm
Wafer thickness range	100 μm – 1 mm
Accuracy	± 0.25 μm
Resolution	0.125 μm

4.7 ELECTRICAL IMPEDANCE TOMOGRAPHY

Electrical impedance tomography is primarily a technique that is used in biomedical applications where the resistivity of the human body is inferred from surface electrical measurements, (the resistivity of organs in the body can vary by a factor of ~ 200 making this a very powerful technique). The same technique can also be applied to wafer characterisation [42-43].

In the method developed by Barber and Brown [44] a number of electrodes are equally spaced around the region to be investigated. A current is introduced between a pair of adjacent electrodes and the resulting potential difference can be measured between all the other pairs of adjacent electrodes. By in turn introducing a current between the other electrodes a resistivity map of the area of interest can be produced. The size and spacing of the electrodes will limit lateral resolution (the probe size was around 100 μm in the example in [42]). The electrodes are also sensitive to positional and contact errors.

In the production of semiconductor devices, knowledge of the electrical properties of the wafer is very important. Variations in resistivity of less than 0.5% across a whole wafer are now routinely achieved. Assuming a uniform resistivity to within the 0.5%, electrical impedance tomography could be used to infer wafer thickness across the wafer. It is likely that a calibrated reference artefact would be required to provide a traceable absolute thickness measurement.

Electrical impedance tomography is a contact method and may be practically challenging to scale down to the dimensions of an individual MEMS device. Like the capacitance method described in section 3.5 the technique cannot distinguish individual layers and thicknesses of a multi-layered structure.

5 COMPARISON OF TECHNIQUES

This section gives a brief comparison of the measurement techniques discussed in the previous section in terms of their suitability for the tomographical measurement of MEMS devices. In some cases it is difficult to be exact regarding the capability of a technique in imaging MEMS devices either because the particular application of the technique is relatively novel or because it depends on the specific details of the method used or the sample in question. In section 2.4 the requirements for a MEMS tomography technique were listed. While the technique needs to be as wide ranging and generic as possible, the minimum requirements were specified and quantified to aid comparison.

Table 3 illustrates how the techniques meet each requirement (green = yes; red = no). In many cases it was better to make a judgement on the likelihood of a technique meeting a particular requirement rather than trying to estimate the exact capability of the technique. For instance the precise depth penetration for OCT will depend on the power of the optical source and the

particular sample. However, it can be easily demonstrated that an OCT system can achieve well beyond 200 μm depth penetration in silicon.

Table 3. Comparison of techniques for measuring the tomography of MEMS devices.

	LCI / OCT	Confocal	Spectral reflect.	Ellipsom.	FTIR	Capacit.	EIT
Single sided	Yes	Yes	Yes	Yes	Yes	No	Yes
Non contact	Yes	Yes	Yes	Yes	Yes	No	No
Axial resolution < 1 μm	< 1 μm	< 1 μm	< 1 μm	< 1 μm	< 1 μm	< 1 μm	~ 1 μm
Lateral resolution < 10 μm	10 μm	< 1 μm	< 1 μm	< 1μm	No	No	No
Depth > 200 μm	Yes	Yes	~ 10 μm	~ 10 μm	~ 10 μm	300 μm	Yes
Silicon compatible	Yes	Yes	Yes	Yes	Yes	Yes	Yes
Scan speed (suitable for industrial application)	Yes	No	Yes	Yes	Yes	Yes	No

From Table 3 it can be seen that the two thin film techniques, spectral reflectometry and ellipsometry, while being very powerful are limited by the depth penetration and so will be applicable to a only a small number of MEMS applications. The two electrical techniques, capacitance and electrical impedance tomography, have been successfully applied to the thickness measurement of silicon wafers. Both techniques may be difficult to scale down to the sizes required for individual MEMS devices. In the case of electrical impedance tomography the difficulty of setting up the equipment could make it prohibitive to a production environment. Both methods also measure total thickness and are incapable of resolving the internal structure of a multi–layered device.

The axial resolution of current commercial OCT systems is around 6 μm. However, there are reasonable grounds to believe that this can be improved to the sub-micrometre level. This is discussed in section 7. Confocal microscopy meets almost all of the technical requirements, however, one concern is the time that it would take to scan a 3D volume. A confocal microscope is also much more complex (and expensive) than an OCT instrument.

In summary LCI/OCT is the best-suited technique for the measurement of wafer thickness in MEMS structures. Confocal microscopy is a viable alternative but the simplicity and

availability of OCT made it the more attractive option. For instance OCT offers the opportunity to build or customise an instrument specifically for a MEMS application.

6 OPTICAL COHERENCE TOMOGRAPHY

This section will now give a brief overview of OCT including its different modalities. It will conclude by considering a range of commercially available instruments. Some OCT images taken of a MEMS device are included by way of a proof of concept.

6.1 OVERVIEW

Optical coherence tomography is a rapidly growing technology and has been successfully applied as a non-invasive, non-destructive imaging technique to a wide range of biomedical applications including ophthalmology.

The technique relies on interference between a split and later recombined broadband optical field [45-46]. The basic system consists of a Michelson interferometer with a broadband source (see Figure 14). When the optical path length from a reflection in the sample matches the optical path length in the reference arm to within the coherence length of the source an interference signal is produced. By scanning the mirror in the reference arm, reflections at different layers within the sample can be detected. This is the basic concept of time domain OCT (TD-OCT). A complete thickness profile of the sample is obtained during a single scan in the z direction (also known as an A-scan) by recording the reference mirror position for all successive null optical path differences (OPDs). The A scan is then repeated to build up a two or three-dimensional image. The frequency output can also be measured and using a Fourier transform can yield the same depth information. This is known as frequency or Fourier domain OCT (FD-OCT) – see 6.3.

It is worth noting that OCT is an absolute measurement method. No thickness artefact is required. Moreover, local thickness measurements are independent of the wafer's bow or warp. OCT measures optical thickness, and so the refractive index of the medium is required to calculate the physical thickness. There has been some work on methods that will simultaneously measure the optical thickness and refractive index [47].

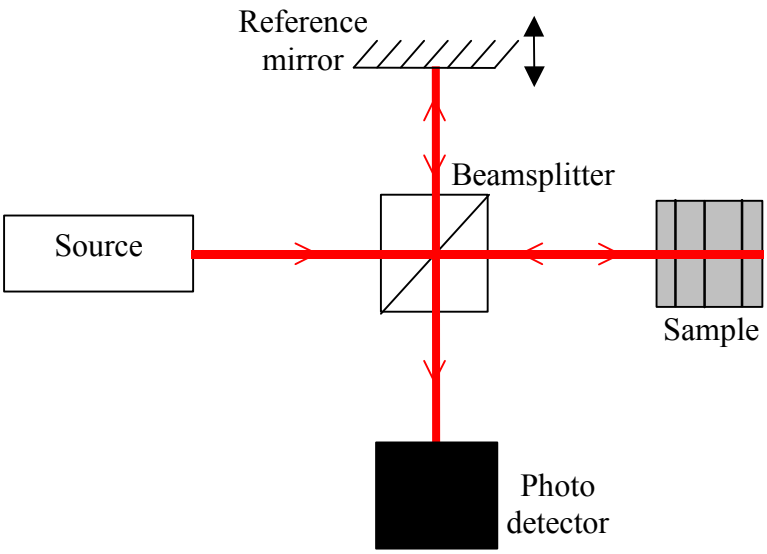

Figure 14. A time-domain OCT system. The reference mirror can be displaced.

6.2 TIME-DOMAIN OPTICAL COHERENCE TOMOGRAPHY

By translating the reference mirror of the interferometer along its optical axis, any boundary formed by two layers of different refractive indices in the sample can be detected. The polychromatic reflection at the boundary will interfere with the polychromatic reflection at the reference arm, hence producing a measurable modulation of intensity [48-51].

The constitution of the interference signal at the detector is explained with the convolution theorem and Fourier analysis. A polychromatic source with a Gaussian intensity spectral distribution of central frequency f_0 and full width at half maximum (FWHM) Δf can also be understood as the convolution product of a zero-centred Gaussian (of the same FWHM) with a Dirac impulse function located at frequency f_0. The Wiener–Khinchin theorem states that the power (or intensity in this case) spectral density of a process is the Fourier transform of its autocorrelation. Reciprocally, the inverse Fourier transform (IFT) of the Gaussian source leads to a time-domain autocorrelation function, which is the standard product of a zero-centred Gaussian distribution of FWHM Δf by a monochromatic carrier of frequency f_0. The Gaussian envelope has the effect of gating the carrier, hence the short temporal coherence of the source. The autocorrelation envelope is also known as the coherence function of the source.

The polychromatic interference equation takes the shape:

$$I = I_R + I_S + 2\sqrt{I_R I_S}\cos(2\pi f_0 \tau)\exp-\left[\frac{\pi \Delta f \tau}{2\sqrt{\ln 2}}\right]^2 \qquad (2)$$

where I is the optical intensity measured at the detector, I_R is the intensity of the signal reflected in the reference arm, I_S is the intensity reflected at (or within) the sample, f_0 is the central frequency of the source, Δf is the FWHM of the Gaussian distribution, and τ is the difference in time-of-flight between the two interferometer arms.

This interference equation is found by taking the time-average of the instantaneous intensity of the sum of the reference and sample signals [46]. Note that the autocorrelation is zero-centred, corresponding to a null time delay (hence a null OPD) between two coherent wave packets each travelling in separate arms of an interferometer. In contrast, a "real" time-domain LCI system would observe the cross-correlation of these coherent wave packets since each of them would traverse and reflect on different media.

The traceability of time-domain OCT is based on the position measurement method of the reference mirror. This forms a radical departure from classical monochromatic interferometry where traceability is propagated by a fringe counter/interpolator system, itself relying on the accurate determination of the laser's central wavelength.

6.3 FREQUENCY-DOMAIN OPTICAL COHERENCE TOMOGRAPHY

OCT can also be performed without displacement of the reference mirror if the interferometer output intensity spectrum is measured. This is effectively a spectral reflectance method [52-57]. The immediate advantage of FD-OCT over TD-OCT is the increased imaging speed as there is no requirement to scan the reference mirror. The light reflected from all layers of the sample contributes at once to the image. The basic setup is shown in Figure 15.

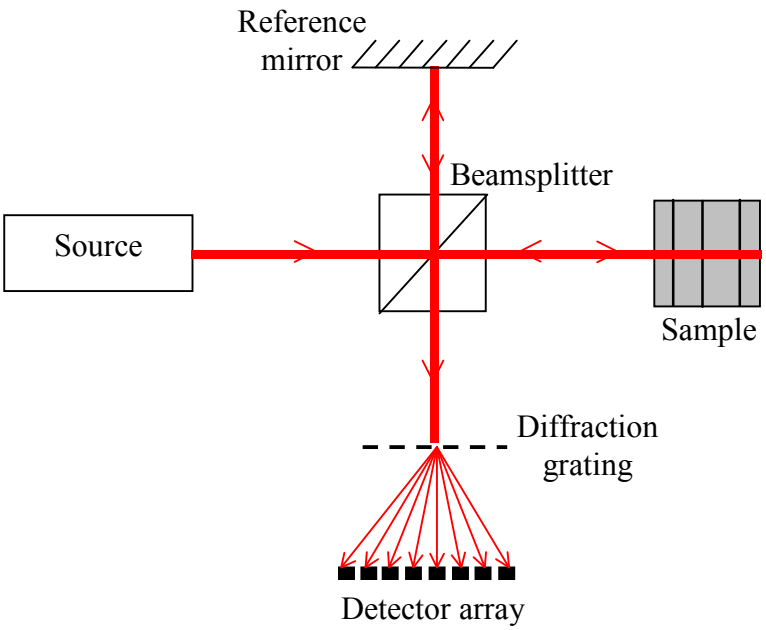

Figure 15. A frequency domain OCT system (FD-OCT). The interferometer output is spectrally dispersed. The reference mirror is not displaced during the measurement.

FD-OCT is based on Fourier decomposition. A broadband source can be treated as a collection of multiple nearly monochromatic frequency bands similar to harmonics. The spectral width of these harmonics is determined by the resolution of the spectrometer. Each harmonic has, by definition, a longer temporal coherence than the complete source, which allows interference to occur between reflections in the sample and the reference arms of the interferometer, somewhat regardless of their OPD.

A particular subset of FD-OCT is swept source OCT [58-62]. Here a tuneable laser whose frequency is continuously scanned can be used enabling the system's spectrometer to be replaced with a single photodiode.

As a result of spectral dispersion at the interferometer output, interference of harmonics with specific central frequencies can be recorded independently of one another. In the same situation, a broadband detector as used in TD-OCT would perceive only a continuous background signal due to the random summation of all the monochromatic interferences.

In this 'multi-chromatic' arrangement, the interference modulation of each harmonic can be treated as if it originated from a single, isolated monochromatic interferometer. The interference function, therefore, assumes the classic shape:

$$I(f,\tau) = I_R(f) + I_S(f) + 2\sqrt{I_R(f)I_S(f)}\cos(2\pi f\tau) \qquad (3)$$

where f is a variable frequency, τ is the delay corresponding to reflection on a particular layer of the sample, $I(f, \tau)$ is the spectral density of interference intensity at frequency f, $I_R(f)$ is the spectral density of intensity in the reference arm at frequency f, and $I_S(f)$ is the spectral density of intensity in the sample arm at frequency f.

The interference function reveals that the position of specific reflective layers in the sample will be encoded in the function plot as fringes of specific 'spectral period'. For example, reflections occurring at locations close to a null OPD will yield a small value of τ and, therefore, produce fringes of long period. The spectral intensity profile measured at the spectrometer is clearly a function of the source profile. The latter can be measured separately (simply by momentarily replacing the sample with a flat mirror) and divided from the equation above to determine the true reflection spectrum of the sample under consideration.

The exact position of each reflection location can be recovered by inverse Fourier transform of the spectral data since the Wiener-Khinchin theorem tells us that the IFT will yield the time-domain cross-correlation function, as if a TD-OCT instrument recorded it. There is, in principle, complete equivalence between the time and frequency domain OCT methods. The determination of layer thickness can, therefore, be obtained using the same time-domain envelope extraction methods and the source's coherence length is perceived in the same way. The axial resolution is equivalent in TD-OCT and FD-OCT, and so is the lateral resolution.

The thickness measurement range in FD-OCT is limited to the spectrometer resolution. As the position of the reflecting layers are encoded in the spectrum by spectral fringes of specific periods, the larger the OPD, the bigger the time-of-flight difference τ and the shorter the period of the spectral fringes. The measurement range limit is reached when the density of detectors in the spectrometer's CCD array becomes insufficient to record spectral fringes without aliasing. To minimise this limitation, the reference mirror must be adequately positioned to provide null OPD at one end of the sample.

Another, perhaps less obvious, range limitation of FD-OCT arises from the fact that the spectrometer will only measure a magnitude spectrum. As a consequence of not resolving the phase spectrum, the inverse Fourier transform of spectral fringes correspond to conjugated Dirac delta functions on either side of the null OPD axis. In other words, it is not possible to know whether a reflection location is situated at location +x or –x of the null OPD axis, which reduces by half the useable depth range.

Another advantage of FD-OCT is the increased signal-to-noise ratio due to spectrometer noise averaging (hence cancellation) resulting from the inverse Fourier transform of the reflection spectrum. Traceability of FD-OCT measurements is ultimately related to the calibration of the spectrometer, which is related to optical frequency standards.

6.4 INSTRUMENT DESIGN

6.4.1 Theory [45-46].

The smallest resolvable thickness is ultimately limited by the separation of two cross-correlation signals, which requires that the reflecting boundaries are at least half a coherence length apart. For a source with Gaussian spectral profile, the coherence length l_c is expressed in vacuum as

$$l_c = \frac{2\ln 2}{\pi} \cdot \frac{\lambda^2}{\Delta\lambda} \tag{4}$$

where λ is the central wavelength of the source and $\Delta\lambda$ is the bandwidth equivalent to the FWHM, (both λ and $\Delta\lambda$ are measured in vacuum).

Provided that the sample contains simple and well-defined layers of materials with significantly different refractive indices, noise due to backscattering at uneven boundaries remains low, and both the carrier and the envelope of the cross-correlation signal can be resolved. In this favourable situation, minimum uncertainty is attached to envelope extraction, implying that the minimal resolvable axial distance can be smaller than half the coherence length of the source, which can be of particular interest in the determination of silicon wafer layer thickness. Reciprocally, highly scattering media will provide reduced axial resolution due to noisy envelope detection.

Unlike classical imaging techniques, OCT provides a complete independence of axial and lateral resolutions. The former is a consequence of the spectral width of the source while the later is related to the numerical aperture (NA) of the delivery and collection optics. Since axial and lateral resolution are completely unrelated, simultaneous high axial resolution and long axial measurement range are possible at sites normally inaccessible with high NA beams. This property is very important for the purpose of imaging MEMS structures. However, high NA is required for high lateral resolution.

The axial resolution is simply expressed as

$$\Delta z = \frac{l_c}{2} \tag{5}$$

where Δz is the minimum resolvable axial distance. The axial resolution equation is somewhat arbitrary since the effective resolution ultimately depends on the ability of the detection algorithm to separate two adjacent coherence peaks.

The lateral resolution is given by

$$\Delta x = 1.22 \frac{\lambda}{2NA} \tag{6}$$

where Δx is the minimum resolvable lateral distance and NA is the numerical aperture of the sample arm focussing lens. This lens has an axial field of view expressed as

$$FOV = \frac{\pi\lambda}{2NA^2} \tag{7}$$

It can be seen that attempting to minimise the lateral resolution is carried out at the expense of the field of view, resulting in a smaller axial measurement range, although this can be compensated by displacing the sample objective lens. By adjusting the focus of the objective lens a series of 2D *en face* slices can be built up through the depth of the sample. This is known as optical coherence microscopy. Alternatively, dynamic focussing can be incorporated into the system to enable high lateral resolution at greater depths. Figure 16 illustrates the trade off between depth of field and lateral resolution.

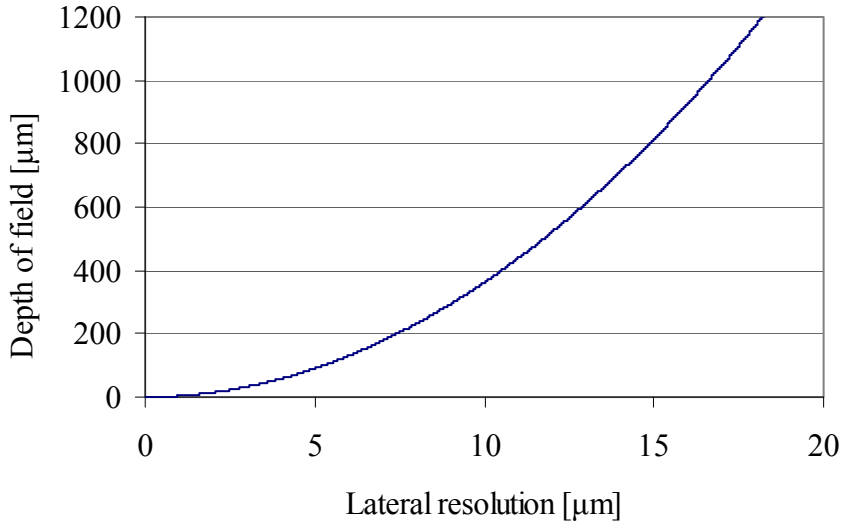

Figure 16. Depth of field against lateral resolution for a 1300 nm source and assuming a refractive index for silicon of 3.5.

Conventional OCT implemented using a single-mode optical fibre mixer is a single-point measurement technique. Three independent scans (axial z scanning by displacement of the reference mirror and lateral xy raster scanning by displacement of the sample relative to the sample objective) are required to obtain a 3D image. Based on the same implementation, the *en-face* [63] technique accelerates the imaging process by repeating lateral (2D) scans for fixed successive positions of the reference mirror, effectively building a 3D image of the sample "slice by slice". In order to improve signal-to-noise ratio, the reference mirror position is oscillated to provide a heterodyne demodulation frequency.

Parallel FD-OCT [64-69] was developed to reduce the scanning to a single axis, thereby increasing the imaging speed, making video-rate imaging possible using a conventional CCD array as the detector instead of a photodiode. In cases where a 2D image is sufficient (for example ophthalmology), parallel FD-OCT can deliver a complete depth-resolved image without any mechanical scanning.

Since a time-domain OCT method is based on peak detection of the cross-correlation envelope, very precise determination of the FWHM and central wavelength of the source is not actually necessary. The only requirement is that the coherence function exhibits certain qualitative properties (a relatively stable, single, centred and narrow peak with minimal side lobes) for the detection algorithm to identify a null OPD.

In most biological OCT applications where the axial resolution is of the order of 10 μm, a compensation technique for dispersion is not required since the effect of group velocity dispersion on coherence length is smaller than the coherence length itself. However, imaging wafers of silicon materials of different forms will require careful compensation if a 1 μm resolution is to be achieved. A range of dispersion compensation techniques are described in the literature [70-76]. These involve placing a compensation material such as a glass block in the reference arm, essentially matching the dispersion effects in the sample arm. Alternatively dispersion can be compensated for in the software analysis using a deconvolution or correlation technique.

6.4.2 Optical sources

Any potential OCT source for applications with MEMS would need to have a central wavelength greater than 1100 nm in order to penetrate silicon. In addition from equation (4) it can be calculated that to achieve a 1 μm axial resolution the source must have a bandwidth of 300 nm. A "Gaussian-like" spectral profile to obtain a simple, symmetrical, single-peaked coherence function (the inverse Fourier transform of the spectral response) is desirable. The power of the source is also an important consideration and will impact on the sample penetration depth. A range of available IR sources are briefly reviewed.

The transformation of LCI techniques into the field of OCT is partially based on recent rapid progress in super-luminescent diode (SLD) technology. An SLD behaves as a laser diode without optical feedback. Super-luminescence occurs when spontaneous emission experiences gain (Amplified Spontaneous Emission or ASE) due to higher injection current. This mode of emission provides only limited time coherence.

SLDs are a popular choice of source for the following reasons:

- Relatively low-cost.
- High power (few tens of milliwatt).
- Broad Gaussian spectral range (up to 100 nm FWHM).
- Large spatial coherence (due to their waveguide structure).
- Large choice of central wavelength (700 nm to 1500 nm).
- Easy coupling with single-mode optical fibres.

The main SLD manufacturers are:

- SuperLum [77].
- Exalos [78].
- Inphenix. [79].

A promising new development in SLD manufacturing is the use of quantum dot InAs/GaAs structures to achieve a broader spectral range. Exalos reports a prototype QD-SLD with a bandwidth of 120 nm at a central wavelength of 1300 nm. This technology is not yet commercially available.

The output of multiple SLDs can be combined together to form an extended spectral response ranging up to 300 nm FWHM. SuperLum has recently introduced a range of multiple SLD sources combining up to four SLDs together with a fibre optic mixer (see Figure 17). The "broadlighter" series of SLDs has a central wavelength ranging from 840 nm to 1430 nm, with an average bandwidth of 200 nm to 300 nm. These sources effectively exhibit a coherence length near or below 1 μm, which is promising for high-resolution OCT.

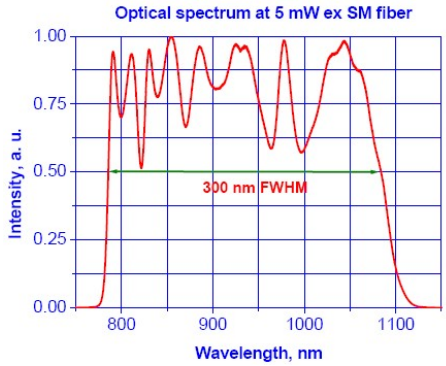

Figure 17. Spectrum of the Superlum broadlighter Q940 source made up of four SLD titanium-doped sapphire IR lasers. (courtesy Superlum)

Titanium-doped sapphire IR lasers use titanium-doped sapphire crystals ($Ti:Al_2O_3$) as their optical gain medium, giving them the possibility to be tuned from 700 nm to 1100 nm, while delivering an output power in the region of a few hundred milliwatts with up to 300 nm FWHM. Spectra-Physics [80] and Femtolasers [81] are two manufacturers of turn-key Titanium-doped sapphire systems.

Thermal sources [82] typically exhibiting the spectral profile of black body radiation are historically categorised as incoherent due to their random emission process over an extended surface area. As a consequence of their large bandwidth extending from the visible region to the

mid-infrared region, their temporal coherence is extremely short (the coherence length typically is less than 1 μm), which is very desirable for OCT. However, their spatial coherence is also extremely short, which is less desirable because it limits the useable coherent power at the detector, resulting in a lower dynamic range, hence a reduced contrast. Despite their large total output power (a few Watts or more), light coupling efficiency to a single mode optical fibre (SMOF) is very poor, making a thermal source unsuitable for OCT application based on a SMOF mixer. In full-field OCT imaging, there is no coupling efficiency limitation but the short spatial coherence of thermal sources can be a hindrance. However, these sources can be exploitable in full-field OCT imaging.

Typical electro-thermal emitters are:

- Tungsten halogen filament.
- Thermoresistive film of amorphous carbon.
- Metal filament (patented design by Metax [82]).

Other sources include swept IR laser, photonic crystal fibre and rare earth-doped optical fibre ring (superfluorescence). Swept IR lasers are required for swept-source OCT (Santec and Thor Labs) [88-95]. Rare earth-doped optical fibre ring sources have maximum bandwidths of 100 nm, which is not enough for sub-micrometre axial resolution.

A range of optical sources for OCT is summarised in Table 4.

Table 4. Examples of light sources for use in OCT – adapted from Fercher [45].

Light Source	λ (nm)	$\Delta\lambda$ (nm)	l_c (μm)	Coherent power (mW)	Reference
SLD	1300	50	15	20	Superlum Diodes Ltd
	1550	45	23.5	10	(2008) [77]
Kerr Lens					
Ti:sapphire laser	810	260	1.5	400	Drexler *et. al*. [84]
Cr: forsterite	1280	120	6	100	Bouma *et. al.* [85]
LED	1240	40	17	0.1	Schmitt *et. al*. [86-87]
Swept IR laser	1325	100	8	12	ThorLabs [88]
ASE fibre sources	1584	44	25	60	www.Photonlines.co.uk (2008) [89]
Superfluorescence					
YB-doped fibre	1064	30	17	40	Bashkansky *et. al*. [90]
Er-doped fibre	1550	80-100	16	100	Bouma *et. al.* [85]
Tm-doped	1800	80	18	7	Bouma *et. al*. [91]
Photonic crystal fibre	1300	370	2.5	6	Hartl *et. al.* [92] Povazay *et. al.* [93]
Thermal tungsten halogen	880	320	1.1	0.0002	Fercher *et. al*. [96] Vabre *et. al.* [94]

6.4.3 Commercially available systems

In the last few years a number of commercially available OCT systems have appeared on the market to meet the demand in the biomedical field [88, 95-97]. Three commercial systems were reviewed as part of this project together with a two custom made systems, designed and manufactured by the Photonics Group at NPL, for use in medical imaging.

There were two aspects to this part of the project, firstly to decide on the design best suited for imaging MEMS devices and secondly to actually image a MEMS sample as a proof of concept and to see what was practically achievable.

In recent years FD-OCT has become the mode of choice. Of the three commercial systems reviewed - Santec, Thor Labs and Michelson Diagnostics (see Figure 18) – all three used swept source FD-OCT. FD-OCT offers scanning speed advantages and in bio-medical or process environments where the sample may not be perfectly still, this is advantageous. The swept source offers benefits in the system design removing the need for a spectrometer.

Figure 18. Three commercial swept source OCT systems. From left, Thor Labs, Michelson Diagnostics, Santec. (Courtesy Thor Labs, Michelson Diagnostics and Santec)

Thor Labs quote the following specifications for their 1300 nm swept source OCT instrument (see Table 5). This particular instrument raster scans the surface to build up a 3D image from the individual A-scans.

Table 5. Specifications for the Thor Labs 1300 nm swept source OCT system.

	1300 nm Swept Source OCT
Optical Specifications	
Centre Wavelength	1325.0 nm
3 db Spectral Bandwidth	100 nm
Imaging Specifications	
Axial Resolution	12.0 μm
Lateral Resolution	20.0 μm
Max Imaging Depth	3.0 mm
Max Imaging Width	10.0 mm
A-Scan Rate	16.0 kHz
Imaging Speed	25 fps

At the time of writing the cost of the Thor Labs instrument is £ 38,000 making it very cost effective when compared to the cost of designing and building an instrument from first principles. Thor Labs also supply a range of OCT components making it possible to assemble a customised instrument relatively easily.

6.5 IMAGING A MEMS SAMPLE

A MEMS pressure sensor produced by GE Sensing as described in section 2 was imaged on each of the three commercial instruments discussed in this section to see what was achievable. All three instruments were able to successfully image the device and in each case some of the sub-structure could be identified. From the output files a movie could be produced and any number of images slicing across the sample in any desired plane. The benefit of scanning the whole sample was apparent as it helped in the identification of specific layers. The images also contained ghosting produced from multiple scattering and with only a single A scan it may be difficult to distinguish the real structure.[2]

Two images produced from the Santec instrument are shown in Figure 19. The images show distinctly the separate layers throughout the sample. It should be remembered that the instrument was configured for imaging biological samples where the reflected signal is much weaker. It should be possible to optimise the system for MEMS and to improve the clarity of image throughout the depth of the sample. For instance the strong reflection from the top surface of the MEMS device can dominate and suppress other reflections in the data analysis. It

[2] A one-dimensional scan in one lateral position through the depth of the sample is known as an A-scan. If the sample is scanned in one direction across the surface, then a two-dimensional slice known as a B-

took around 60 seconds for the system to image the sample, which is approximately a 2 mm x 2 mm x 2 mm volume.

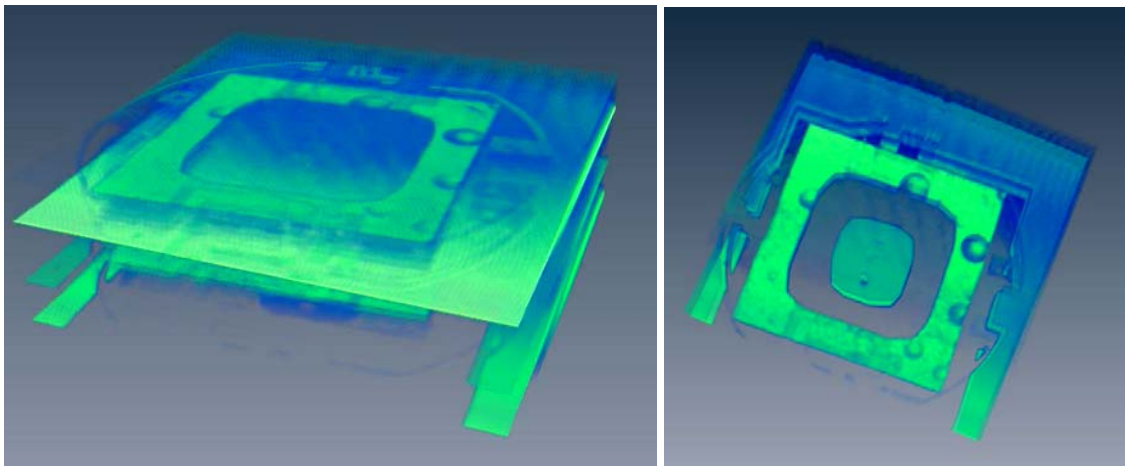

Figure 19. Two images of an RPT pressure sensor taken on an OCT swept source instrument (Santec).

One limit on imaging samples is data handling and data storage. A typical B scan for a 6 mm x 2 mm slice with a 5 μm axial resolution typically creates a 10 Mb file. A 3D sample with a sequence of B scans at 20 μm spacing over a 6 mm length would create a 3 Gb file. Any increase in the resolution yields a proportional increase in file size. Data handling can set a limit on the scan rate rather than the physical speed of the instrument. One option would be to have some kind of buffering setup, particularly if defect detection was the main requirement.

7 POTENTIAL DEVELOPMENT OF OCT FOR MANUFACTURED STRUCTURES

Close comparisons can be made between OCT and coherence scanning interferometry The principle is broadly speaking, the same, with the exceptions that CSI works in the visible part of the spectrum and is generally concerned with imaging surfaces. It is interesting to note that CSI instrument manufacturers routinely quote sub-nanometre axial resolutions. This is made possible by resolving below the coherence length of the source.

There are some well-documented limitations to CSI as a topographical technique [98-100]. High aspect ratio structures can be difficult to image. In particular batwing effects can be observed when looking at steps due to diffraction, and gradients such as v-grooves can either be outside the acceptance angle of the instrument or produce spurious images due to multiple reflections (algorithms for CSI are based on linear scattering models).

---

scan is imaged. By raster scanning across the surface a three–dimensional volume known as a C-scan can be imaged.

7.1 IMPROVED DEPTH RESOLUTION FOR THE TOMOGRAPHY OF ENGINEERED STRUCTURES

It should be possible to improve on coherence length limited axial resolutions for manufactured structures. Engineered surfaces will produce stronger reflections and better signal/noise ratios than biological tissue and often there will be some prior knowledge about the structure such as an engineering drawing. Using an iterative approach, the gathered data can be refined to optimise resolution. While it is very likely that a surface can be located positionally to a sub coherence length resolution, it is still very difficult to precisely locate surfaces that are within a coherence length of each other. However, it is most likely that thin layers will be located on the surface and can be determined using thin film techniques rather than tomography.

7.2 OCT FOR HIGH ASPECT RATIOS

Another possible application of OCT is in measuring difficult to measure surface features on engineered structures, such as HARS. Often these features will be unmeasurable or will produce false results due to multiple scattering. A feature of OCT is that an optical thickness is obtained which is converted to a physical thickness through knowledge of the refractive index of the medium. Using reverse engineering this optical thickness information could be used to extract information on the surface to be measured.

With the assumption that reflections can be obtained from the lower surface of the sample, the perceived position of the lower surface will be dependant on the amount of silicon the light has passed through. If there is some knowledge of the lower surface then this information can be used to calculate the topography of the upper surface by knowing the thickness of the silicon. If the lower surface was perfectly flat then an OCT instrument would see a mirror image of the upper surface in the measured image of the lower surface.

Some knowledge of the bottom or datum surface is a perquisite for this method. Any roughness or imperfections in this surface will result in an error in the surfaces to be calculated. Sub-micrometre resolutions will be required to successfully image some of the HAR structures commonly seen in MEMS devices.

One necessary consideration is the refraction of the light through the sample. This will cause significant measurement errors, as the refractive index of the silicon is considerably different to the refractive index of air. However if the refractive index of the sample was known it may be possible to correct for refraction. Alternatively by imaging the sample from different angles it may be possible to mathematically extract both refractive index and dimensional information. If

the surface of the silicon was sufficiently rough it might be that a small fraction of the light would be transmitted directly through the sample.

8 SUMMARY AND RECOMMENDED ACTIONS

This project was tasked with identifying a method of measuring wafer thickness and to then develop an instrument for the task. Optical coherence tomography was chosen as the best suited method and some simple tests using existing commercial instruments proved that OCT was indeed a suitable technique.

None of the three commercial instruments looked at during this project (nor any others to the authors knowledge) were capable of achieving the sub-micrometre axial resolution stated as a requirement in chapter 2. The limitation from a hardware perspective is due to the bandwidth of the optical source. Furthermore it does not seem that there are commercial sources available operating in the required IR region that can significantly improve on those currently used in OCT instrumentation.

It is in the last few years that a number of commercial instruments have become available driven by the rapid take up of OCT as an imaging technique in the biomedical field. Indeed the Photonics Group at NPL, having built several OCT instruments for medical imaging, have recently purchased a commercial system, as it is no longer cost effective to design and produce a one-off instrument. With this in mind it is difficult to see what could be gained in designing and building an OCT instrument to measure wafer thickness. The market need is starting to be addressed by industry and this is a trend that will continue over the next few years. At present there isn't a strong enough demand in the MEMS industry within the UK to justify NPL purchasing an OCT instrument. Furthermore even if there was a demand it is not clear where NPL would add value to what instrument manufacturers are already providing.

One exciting opportunity for development that has emerged is image-processing software for LCI. It is believed that the development of suitable software will enable sub-micrometre axial resolutions to be achieved for OCT on manufactured structures. An iterative approach will also allow more complex structures including high aspect ratios and sidewalls to be imaged. The work will also have relevance not just to OCT but also to CSI and surface measurement. In addition there is already interest from an OCT instrument manufacturer who would like to introduce OCT to non-biomedical sectors.

It is the recommendation of this report to propose a project on imaging processing software for

LCI, encompassing the initial requirement to measure wafer thickness. Working with OCT manufacturers and existing hardware, a collaborative project has potential to add considerable value in the field.

9 ACKNOWLEDGEMENTS

The authors would like to acknowledge the financial support of the National Measurement System Directorate of the UK Department of Innovation, Universities and Skills. The authors would like to thank Professor Jeremy Coupland of Loughborough University, Russell Craddock of GE Sensing, David Heard of Santec, Rebecca Eley of BAE Systems, and Pete Tomlins and Matthew Tedaldi of the National Physical Laboratory. Finally the authors would also like to thank Francois Maletras formerly of the National Physical Laboratory for his contribution to this report.

10 REFERENCES

[1] Reilly S P, Leach R K, Cuenat A, Awan S A and Lowe M 2006 *Overview of MEMS sensors and the metrology requirements for their manufacture* NPL Report DEPC-EM 008 (National Physical Laboratory)

[2] Ptyputniewicz R J, Heefti P, Klempner A R, Marinis R T and Furlong C 2004 Hybrid methodology for the development of MEMS *Proc. ICEM12 – 12th International conference on experimental mechanics*

[3] Rapp D *Thermo-Optical properties of silicon* Website:www.gps.caltech.edu/genesis/Thermal-Coll.html

[4] Becker M and Fan Y 1949 Optical properties of semiconductors. III. Infra-red transmission of silicon *Phys. Rev.* **76** 1531-32

[5] Stumpf W 2001 *Investigation and simulation of the optical properties of doped silicon* http://w3.ub.uni-konstanz.de/v13/volltexte/2004/1197//pdf/wstumpf_eos.pdf *(University of Constance)*

[6] de Groot P and Colonna de Lega X 2004 Signal modelling for low-coherence height-scanning interference microscopy *Appl. Opt.* **43** 4821-30

[7] Colonna de Lega X and de Groot P 2005 Optical topography measurement of patterned wafers *AIP Conference Proc.* **788** 432-6

[8] Wyant J C 2002 White light interferometry *Proc. SPIE* **4737** 98-107

[9] Blunt R 2006 White light interferometry – a production worthy technique for measuring surface roughness on semiconductor wafers *CS Mantech Conf. Vancouver,* 59-62

[10] de Groot P, Colonna de Lega X, Kramner J and Turzhitsky M 2002 *Appl.Opt.* **41** 4571-78

[11] de Groot P 1994 Surface profiling by frequency-domain analysis of white light interferograms *Proc. SPIE* **2248** 101-4

[12] de Groot P 1993 What is frequency domain analysis? *Zygo R&D Technical Bulletin*

[13] Deck L 2003 Fourier-transform phase–shifting interferometry *Appl.Opt.* **42** 2354-65

[14] Mansfield D, 2006 The distorted helix: thin film extraction from white light interferometry *Proc. SPIE* **6186** 61860O

[15] Mansfield D, 2006 Thin film extraction from scanning white light interferometry Proc *ASPE Annual Meeting, Monterey, California* **39** 23-6

[16] Poilane C and Sandoz P 2006 Thickness measurement of nontransparent free films by double-side white-light interferometry: calibration and experiments *Rev. Sci. Instrum.* **77** 055102

[17] de Groot P, Beigen J, Colonna de Lega X and Grigg D 2002 Optical interferometry for measurement of the geometric dimensions of industrial parts *Appl.Opt* **41** 3853-60

[18] Claxton N S, Fellers T J and Davidson MW Laser scanning confocal microscopy *Website:www.olympusconfocal.com/theory/LSCMIntro.pdf viewed on the 19th March 2008*

[19] Website: www.olympus.co.uk

[20] Website: www.nikoninstruments.eu

[21] Website:www.zeiss.co.uk

[22] Website:www.leica.com

[23] Tiziani H J and Uhde H, 1994 Three dimensional image sensing by chromatic confocal microscopy *Appl. Opt.* **33** 1838-43

[24] Cha S, Lin P, Zhu l, Sun P and Fainman Y, 2000 Nontranslational three-dimensional profilometry by chromatic confocal microscopy with dynamically configurable micromirror scanning *Appl. Opt*. **39** 2605-13

[25] Koklu F H, Meydbray Y, Behringer E R, Quesnel J I, Karabacak D, Ippolito S B, Goldberg BB and Unlu M S 2006 Subsurface imaging with widefield and confocal numerical aperture increasing lens microscopes *Proc. of IEEE Lasers and Electro-Optics Society* 695-6

[26] Lu W, Sun J and Pei Z, 2006 Subsurface damage measurement in silicon wafers with cross-polarisation confocal microscopy *Int. J. Nanomanufacturing* **1** 272-82

[27] Azzam R M A and Bashaa N M 1987 *Ellipsometry and polarized light* (North-Holland publishing company)

[28] Tompkins G G and Irene E A 2005 *Handbook of ellipsometry* (Springer-Verlag)

[29] Yacoot A and Leach R K 2007 *Review of x-ray and optical thin film measurement*

methods and transfer artefacts NPL report DEPC-EM 013 (National Physical Laboratory)

[30] Website:www.jawoollam.com

[31] Pickering C 2001 Optical characterization techniques for process monitoring *Surf. Interface Anal.* **31** 909-14

[32] Sopori B L 1988 Principle of a new reflectometer for measuring dielectric film thickness on substrates of arbitrary surface characteristics *Rev. Sci. Instrum* **59** 725-7

[33] Sopori B, Zhang Y, Faison R and Madjdpour J 2001 Principles and applications of reflectometry in PV manufacturing *NCPV Program Review Meeting, Lakewood, Colarado*

[34] Sopori B, Zhang Y and Chen W 1999 Process monitoring in solar cell manufacture *9th Workshop on Crystalline Silicon Solar Cell Materials and Processes, Colorado Aug 9-11*

[35] Sopori B, Amieva J, Butterfield B and Li C 2005 Rapid mapping of AR coating thickness on Si solar cells using GT-Fabscan 6000 *31st IEEE Photovoltaic Specialists Conference and Exhibition, Florida, USA*

[36] Sopori, 2004 Reflectance spectroscopy: rapid quantitative measurements in commercial production of Si.solar cells *DOE Solar Energy Technologies Program Review Meeting Oct 25-28, Denver, Colorado*

[37] Rosencwaig A, Opsal J, Willenborg D L, Kelso S M and Fanton J T 1992 Beam profile reflectometry: a new technique for dielectric film measurements. *Appl. Phys. Lett.* **60** 1301-3

[38] Leng J M, Sidorowich J J, Yoon Y D, Opsal J, Lee B H, Cha G, Moon J and Lee S I 1997 Simultaneous measurement of six layers in a silicon on insulator film stack using spectrophotometry and beam profile reflectometry *J. Appl. Phys.* **81** 3570-78

[39] Fanton J T, Opsal J, Willenborg D L, Kelso S M and Rosencwaig A 1993 Multiparameter measurements of thin films using beam-profile reflectometry *J. Appl. Phys.* **73** 7035-40

[40] Website:www.thermo.com

[41] Website:www.mtiinstruments.com.

[42] Djamdji F, Gorvin A, Freeston I, Tozer R, Mayes I and Blight S 1996 Electrical impedance tomography applied to semiconductor wafer characterization *Meas Sci. Technol.* **7** 391-5

[43] Kruger M, Poolla K and Spanos C 2002 Electrical impedance tomography based sensors for semiconductor manufacturing. *Proc. American Control Conference, Anchorage, Alaska*

[44] Barber D C and Brown B H 1984 Applied potential tomography *J. Phys. E: Sci. Instrum*

17 723-33

[45] Tomlins P H and Wang R K 2005 Theory, developments and applications of optical coherence tomography *J Phys. D: Appl. Phys.* **38** 2519-35

[46] Fercher A F, Drexler W, Hitzenberger C K and Lasser T 2003 Optical coherence tomography – principles and applications. *Rep. Prog. Phys.* **66** 239-303

[47] Tomlins P H, Tedaldi M, Ferguson R and Wang R 2006 Stereoscopic optical coherence tomograpghy in the frequency domain for refractive index sensitive imaging *Proc. SPIE.* **6627**

[48] Wilhelm R, Courteville A and Garcia F 2006 A novel, low coherence fibre optic interferometer for position and thickness measurements with unattained accuracy *Proc. SPIE* **6341**

[49] Wilhelm R, Courteville A, Delaveau M and Garcia F 2005 Non-contact in-process metrology using a high accuracy low coherence interferometer *Proc. Laser Metrology and Machine Performance VII* 534-544

[50] Ko T H, Adler D C and Fujimoto J G 2004 Ultrahigh resolution optical coherence tomography imaging with a broadband superluminescent diode light source *Opt. Express* **12** 2112-9

[51] Maruyama H, Inoue S, Mitsuyama T, Ohmi M and Haruna M 2002 Low-coherence interferometer for the simultaneous measurement of refractive index and thickness *Appl. Opt.* **41** 1315-22

[52] Leitgeb R A, Drexler W, Povzay B, Hermann B, Sattman H and Fercher A F 2005 Spectroscopic Fourier domain optical coherence tomography: principle, limitations and applications *Proc. SPIE.* **5690** 151-8

[53] Tomlins P H and Wang R K 2006 Simultaneous analysis of refractive index and physical thickness by Fourier domain optical coherence tomography. *IEE Proc.-Optoelectron* **153** 222-8

[54] Fercher A F, Hitzenberger C K, Kamp G and El-Zaiat S Y 1995 Measurement of intraocular distances by backscattering spectral interferometry *Opt. Commun.* **117** 43-8

[55] Vakhtin A B, Kane D J, Wood W R and Peterson K A 2003 Common–path interferometer for frequency-domain optical coherence tomography *Appl. Opt.* **42** 6953-8

[56] Grajciar B, Pircher M, Fercher A F and Leitgeb R A 2005 Parallel Fourier domain optical coherence tomography for in vivo measurement of the human eye *Opt. Express* **13** 1131-7

[57] Costantino S and Martinez O E 2003 Wide band interferometry for thickness measurement *Opt. Express* **11** 952-6

[58] Huber R, Wojtkowski M, Taira K and Fujimoto J G 2005 Amplified, frequency swept

lasers for frequency domain reflectometry and OCT imaging: design and scaling principles *Opt. Express* **13** 3513-28

[59] Huber R, Taira K, Wojtkowski M, Ko T H, Fujimoto J G and Hsu K 2005 High speed frequency swept light source for Fourier domain OCT at 20 kHz A-scan rate *Proc. SPIE* **5690** 96-100

[60] Maheshwari A, Choma M A and Izatt J A 2005 Heterodyne swept-source optical coherence tomography for complete complex conjugate ambiguity removal *J. Biomed. Opt* **10** 64005

[61] Choma M A, Hsu K, and Izatt J A, 2005 Swept source optical coherence tomography using a 1300 nm ring laser source *J. Biomed. Opt.* **10** 044009

[62] Nielsen F D, Thrane L, Black J, Hsu K, Bjarklev A and Andersen P E 2005 Swept-wavelength source in the 1 μm range *Opt. Express* **13** 4096-106

[63] Wiesauer K, Pircher M, Götzinger E, Bauer S, Engelke R, Ahrens G, Grützner G, Hitzenberger C K and Stifter D 2005 En-face scanning optical coherence tomography with ultra-high resolution for material investigation *Opt. Express* **13** 1015-24

[64] Dubois A, Grieve K, Moneron G, Lecaque R, Vabre L and Boccara C 2004 Ultrahigh-resolution full-field optical coherence tomography *Appl. Opt.* **43** 2874-83

[65] Grieve K, Dubois A, Simonutti M, Paques M, Sahel J, Le Gargasson J and Boccarra C 2005 In vivo anterior segment imaging in the rat eye with high speed white light full-field optical coherence tomography *Opt. Express* **13** 6286-95

[66] Moreau J, Loriette V and Boccara A 2003 Full-field birefringence imaging by thermal-light polarization-sensitive optical coherence tomography *Appl. Opt.* **42** 3800-10

[67] Dubois A, Moneron G, Grieve K and Boccarra A 2004 Three-dimensional cellular-level imaging using full-field optical coherence tomography *Phys. Med. Biol.* **49** 1227-34

[68] Marks D, Ralston T, Boppart S and Carney P 2007 Inverse scattering for frequency-scanned full-field optical coherence tomography *J. Opt. Soc. Am. A* **24** 1034-41

[69] Oh W, Bouma B, Iftimia N, Yun S, Yelin R and Tearney G 2006 Ultrahigh-resolution full-field optical coherence microscopy using InGaAs camera *Opt. Express* **14** 726-35

[70] Fercher A F, Hitzenberger C K, Sticker M, Zawadzki R, Karamata B and Lasser T 2002 Dispersion compensation for optical coherence tomography depth-scan signals by a numerical technique *Opt. Commun.* **204** 67-74

[71] Liu B, Macdonald E, Stamper D and Brezinski M 2004 Group velocity dispersion effects with water and lipid in 1.3 μm optical coherence tomography system *Phys. Med. Biol.* **49** 923-30

[72] Fercher A F, Hitzenberger C K, Sticker M and Zawadzki R 2001 Numerical dispersion compensation for partial coherence interferometry and optical coherence tomography

Opt. Express **9** 610-15

[73] Gao W 2007 Dispersion properties of grating-based rapid scanning optical delay lines *Appl. Opt.* **46** 986-92

[74] Chan K, Devaraj B, Yamada M and Inaba H 1997 Coherent detection techniques in optical imaging of tissues *Phys. Med. Biol.* **42** 855-67

[75] Tomlins P H, Palin W, Shortall A and Wang R 2007 Time-resolved simultaneous measurement of group index and physical thickness during photopolymerization of resin-based dental composite *J. Biomed. Opt.* **12** 014020

[76] Tomlins P H and Wang R 2006 Matrix approach to quantitative refractive index analysis by Fourier domain optical coherence tomography *J. Opt. Soc. Am. A.* **23** 1897-907

[77] Website:www.superlumdiodes.com

[78] Website:www.exalos.com

[79] Website:www.inphenix.com

[80] Website:www.newport.com

[81] Website:www.femtolasers.com

[82] Fercher A F, Hitzenberger C K, Sticker M, Moreno-Barriso E, Leitgeb, Drexler W and Sattmann H 2000 A thermal light source technique for optical coherence tomography. *Opt. Commun* **185** 57-64

[83] Website: www.metax.co.uk/infrared_source.htm

[84] Drexler W, Morgner U, Kartner F, Pitris C, Boppart S, Li X, Ippen E and Fujimoto J 1999 In vivo ultrahigh-resolution optical coherence tomography. *Opt. Lett.* **24** 1221-3

[85] Bouma B, Tearney G, Bilinsky I, Golubovic and Fujimoto J 1996 Self-phase-modulated Kerr-Lens mode-locked Cr:forsterite laser source for optical coherence tomography *Opt. Lett.* **21** 1839-41

[86] Schmitt J and Knüttel A 1997 Model of optical coherence tomography of heterogeneous tissue *J. Opt. Soc. Am A* **14** 1231-42

[87] Schmitt J, Lee S and Yung K 1997 An optical coherence microscope with enhanced resolving power in thick tissue *Opt. Commun.* **142** 203-7

[88] Website:www.thorlabs.com

[89] Website:www.photonlines.com

[90] Bashkansky M, Duncan M, Goldberg L, Koplow J and Reinjes J 1998 Characteristics of a Yb-doped superfluorescent fibre source for use in optical coherence tomography *Opt. Express* **3** 305-10

[91] Bouma B, Nelson L, Tearney G, Jones D, Brezinski M and Fujimoto J 1998 Optical coherence tomographic imaging of human tissue at 1.55 mm and 1.81 mm using Er- and Tm-doped fiber sources *J. Biomed. Opt*. **3** 76-9

[92] Hartl I, Li X, Chudoba C, Ghanta R, Ko T, Fujimoto J, Ranka J and Windeler R 2001 Ultrahigh-resolution optical coherence tomography using continuum generation in an air-silica microstructure optical fibre *Opt. Lett.* **26** 608-10

[93] Povazay B et al 2002 Submicrometer axial resolution optical coherence tomography *Opt. Lett.* **27** 1800-2

[94] Vabre L, Dubois A and Boccara A 2002 Thermal-light full field optical coherence tomography. *Opt. Lett.* **27** 530-2

[95] Website: www.santec.com

[96] Website: www.md-ltd.co.uk

[97] Website: www. fogale.fr/pages/index.php

[98] Gao, F, Leach, R K, Petzing, J and Coupland J M 2008 Surface measurement errors using commercial scanning white light interferometers *Meas. Sci. Technol.* **19** 015303

[99] Gao F, Petzing J N, Coupland J M and Leach R K 2007 Measurement of structured surfaces using stylus AFM and optical methods *Proc. 11th International Conf. Metrology and Properties of Engineering Surfaces, Huddersfield University, UK* 363-4

[100] Gao F, Coupland J M and Petzing J, 2006 V-groove measurement with a white light interferometer *Photon06 (Manchester, 4-7 Sept*.)